Phase Equilibria in an Amphiphilic Peptide–Phospholipid Model Membrane by Deuterium Nuclear Magnetic Resonance Difference Spectroscopy†

J. C. Huschilt,‡ R. S. Hodges,§ and J. H. Davis*,‡

Biophysics Interdepartmental Group and Guelph-Waterloo Program for Graduate Work in Physics, University of Guelph, Guelph, Ontario, Canada N1G 2W1, and Department of Biochemistry and Medical Research Council Group in Protein Structure and Function, University of Alberta, Edmonton, Alberta, Canada T6G 2H7

Received June 29, 1984

ABSTRACT: Deuterium nuclear magnetic resonance difference spectroscopy has been used to determine the phase boundaries of the fluid and gel phases of a synthetic amphiphilic peptide–phospholipid model membrane system. Between these phase boundaries lies a simple two-phase region containing fluid and gel phase domains. The accurate measurement of these phase boundaries by ^2H nuclear magnetic resonance difference spectroscopy permits the quantitative description of the partitioning of the membrane components between the phases as the temperature is varied. The two similar peptides, one having a hydrophobic core of 16 leucines and the other having 24, both result in a broad two-phase region at temperatures below the pure lipid melting temperature. The shorter peptide closely matches the hydrophobic thickness of the bilayer fluid phase so that there is no increase in hydrocarbon chain order as peptide concentration is increased. The longer peptide results in a linear increase in chain order with peptide concentration. The observed phase boundaries and the influence of the peptide on lipid hydrocarbon chain order within the two phases are indicative of nonideal mixing. The small but significant difference between the two systems suggests a contribution to the lipid–peptide interaction which depends on the degree of mismatch between the length of the hydrophobic part of the peptide and the bilayer thickness. The extension of the techniques to reconstituted protein–lipid systems is straightforward. The description of the partitioning of protein phases can then be compared to the temperature dependence of protein activity to determine the influence of the physical state of the membrane on protein function.

How protein–lipid interactions influence membrane function is a question of fundamental importance. These interactions may, on the one hand, provide a means of modulating protein function through changes in membrane lipid properties or, on the other hand, provide a means of controlling lipid bilayer physical properties through changes in membrane proteins. At the molecular level, protein–lipid interactions may manifect themselves as local or site-specific perturbations. Accordingly, many investigations of protein–lipid interactions have been directed toward finding examples of a lipid specificity for protein function (Brophy et al., 1984; Griffith et al., 1982; Sixl et al., 1984) while other have concentrated on studying the changes in lipid orientational order and dynamics induced by the presence of protein in the bilayer (Paddy et al., 1981; Deese et al., 1981; Bienvenue et al., 1982; Jacobs & Oldfield, 1981; Davis, 1983).

Electron paramagnetic resonance (EPR)[1] spin-label experiments on reconstituted membranes (Jost et al., 1973) identified a layer of lipid at the protein periphery through its increased orientational order (on the EPR time scale 10^{-8}–10^{-9} s). Nuclear magnetic resonance (NMR) experiments on similar systems (Paddy et al., 1981; Bienvenue et al., 1982; Kang et al., 1979; Oldfield et al., 1978) can be interpreted in terms of a single average environment on the much longer NMR time scale (10^{-3}–10^{-6} s). The lifetime of a lipid or spin probe on a specific lattice site within the bilayer, whether near a protein or in a bulk lipid phase, is estimated from diffusion measurements to be on the order of 10^{-8} s so that the lipid molecule can sample a large area of the membrane during the NMR measurement but is "frozen" in position during the EPR measurement (Davis, 1983). The fast motions responsible for the orientational averaging over times shorter than, or on the order of, the EPR time scale seem to be modified when the lipid is in direct contact with a protein, but a specific lipid molecule need not spend any more time in a site near a protein than it does in any other lattice site (Paddy et al., 1981; Davis, 1983).

The local perturbations in molecular motion and orientational order are only one manifestation of the interaction between protein and lipid. A potentially more important effect is the modification of membrane phase equilibria by this interaction. The hydrophobic interaction is primarily responsible for the formation of the lipid bilayer. Integral membrane proteins are obliged to have hydrophobic moieties with lengths which approximately match the hydrophobic thickness of the lipid bilayer. A mismatch between the hydrophobic part of the protein and the membrane thickness would tend to expose either the hydrophobic bilayer interior or the hydrophobic core of the protein to the aqueous medium. To minimize the total free energy of the system, the protein and the lipid bilayer must readjust themselves to a more favorable hydrophobic match (Owicki et al., 1978; Owicki & McConnell, 1979; Mouritsen

† This research was supported by the Natural Sciences and Engineering Research Council of Canada (J.C.H. and J.H.D.) and by the Medical Research Council of Canada (R.S.H.).

* Address correspondence to this author at the Department of Physics, University of Guelph.

‡ University of Guelph.

§ University of Alberta.

[1] Abbreviations: EPR, electron paramagnetic resonance; NMR, nuclear magnetic resonance; DPPC-d_{62}, 1,2-bis(perdeuteriopalmitoyl)-*sn*-glycero-3-phosphocholine; peptide 24, Lys_2-Gly-Leu_{24}-Lys_2-Ala-amide; peptide 16, Lys_2-Gly-Leu_{16}-Lys_2-Ala-amide; T_{2e}, quadrupolar echo decay time.

0006-2960/85/0424-1377$01.50/0

& Bloom, 1984; Davis et al., 1983; McLachlan & Henderson, 1980).

Changes in membrane phase equilibria reflect the changes in the total free energy of the system. The measurement of phase boundaries in binary lipid mixtures and in protein–lipid reconstitutions provides valuable information about the molecular interactions between the components (Mabrey & Sturtevant, 1977; Chapman et al., 1979; Davis et al., 1983; Mouritsen & Bloom, 1984).

To determine the form and relative importance of the different free energies in a thermodynamic model of membrane phase equilibria, one needs to be able to change the characteristic variables. These include not only the temperature and concentration but also the quantities which determine the strength of the various interactions. In the case of the hydrophobic mismatch between proteins and lipids, for example, it is important to be able to vary the amount of the mismatch. This can readily be accomplished by changing the length of lipid hydrocarbon chains and by varying the hydrophobic length of the protein. Systematically modifying the chemical structure of both protein and lipid will facilitate the determination of the character of the protein–lipid interactions.

By the use of synthetic amphiphilic peptides as protein analogues (Davis et al., 1982, 1983; Mouritsen & Bloom, 1984), we avoid many of the problems of large-scale protein preparation, purification, and characterization associated with the use of natural membrane proteins in reconstituted systems. In addition, we enjoy the flexibility of being able to modify the peptide's sequence as well as its length, hydrophobicity, and polarity. Finally, the peptide's small size and simple structure [predominantly α-helical in this instance (Davis et al., 1983)] greatly simplify the interpretation.

Nuclear magnetic resonance, like other spectroscopic techniques, is sensitive to the degree of motional averaging that occurs on the time scale of the experiment. This time scale ranges from about 1 ms to about 10μs for the ^{2}H spectra observed in membrane systems. Motions which are faster than this will reduce the average quadrupolar intteraction if these motions modulate the orientation of the electric field gradient tensor relative to the magnetic field direction. This orientational averaging profoundly influences the NMR spectrum. Because of the inherently microscopic nature of NMR, we must be careful when trying to extract a macroscopic or thermodynamic description of the system from these spectra. In particular, we must ensure that we are observing the equilibrium properties of the system and not dynamic effects which are influenced by our experimental time scale. By carefully performing identical NMR experiments on a series of amphiphilic peptide–phospholipid model membrane samples, we have been able to obtain a consistent, quantitative description of the phase equilibria from the NMR spectra.

After brief descriptions of the peptide and lipid syntheses and the experimental procedures used, we present the results of a detailed study of the phase equilibria of two peptide–phospholipid model membranes. The two peptides, Lys_2-Gly-Leu_N-Lys_2-Ala-amide, used differ only in N, the number of leucines forming the hydrophobic core. Peptide 24 (Davis et al., 1983) has N = 24 leucines while peptide 16 has N = 16 leucines. Two different hydrophobic lengths were used in an effort to investigate the importance of any mismatch between the hydrophobic bilayer thickness and peptide length (Mouritsen & Bloom, 1984; Davis et al., 1983; Lewis & Engelman, 1983; Owicki et al., 1978). We then describe a systematic method for determining phase boundaries for systems exhibiting a region of gel and fluid phase coexistence from ^{2}H NMR spectra. Once phase boundaries have been accurately determined, the significance of peptide–lipid mismatch and the partitioning of the peptide between phases are discussed.

Materials and Methods

The peptides were synthesized on a Beckman Model 990 solid phase peptide synthesizer. The details of peptide synthesis and purification were described previously (Davis et all., 1983).

Peptide 24, the longer of the two peptides, has a hydrophobic core of 24 leucines with hydrophilic amino acids at either end. The complete sequence is Lys_2-Gly-Leu_{24}-Lys_2-Ala-Amide ($K_2GL_{24}K_2A$-amide). Its five positive charges are neutralized by five acetate ions so that the formula weight, including counterions, is 3669.

The shorter peptide, peptide 16, has a core of 16 leucines with the same hydrophilic groups at either end. Its sequence is Lys_2-Gly-Leu_{16}-Lys_2-Ala-amide ($K_2GL_{16}K_2A$-amide), and it also has five acetate counterions so that its formula weight is 2765.

Amino acid analyses were performed on these peptides as described previously (Davis et al., 1983). The results for peptide 24 are the following: concentrated sample, Gly (0.98), Ala (1.07), Lys (3.97), Leu (off scale); dilute sample, Gly (1.02), Ala (1.07), Lys (4.28), Leu (23.64). For peptide 16, the analysis showed the following: Gly (1.02), Ala (1.10), Lys (3.94), Leu (15.94). [Peptide 24 was of the same batch as the second peptide used previously [labeled peptide 2 in Davis et al. (1983).]

The phospholipid 1,2-bis(perdeuteriopalmitoyl)-*sn*-glycero-3-phosphocholine (DPPC-d_{62}) was synthesized in our laboratory according to the procedure described by Gupta et al. (1977) and was from the same batch used in Davis et al. (1983).

The NMR samples were prepared by combining appropriate volumes from a 20 mM solution of DPPC-d_{62} in methanol and a 0.2 mM solution of peptide 24 in methanol, except that the last two samples studied, peptide concentrations x_p = 0.0051 and 0.0149, were made from appropriate dry weights. For peptide 16, the stock solutions were 3 mM DPPC-d_{62} in methanol and 60 μM peptide 16 in methanol. In making these solutions, it was assumed that the deuterated phospholipid had two waters of hydration (Albon & Sturtevant, 1978) so that its formula weight was taken to be 832.

The mixed solution was then gently dried by rotary evaporation and then further dried overnight under vacuum at room temperature.

A typical NMR sample contained about 85 mg of DPPC-d_{62} which, together with the appropriate amount of peptide, was hydrated with, typically, 100 μL (for peptide 24) of phosphate buffer, 50 mM at pH 7.0. (Two early samples of peptide–24 DPPC-d_{62} at peptide concentrations of x_p = 0.0100 and 0.0197 were hydrated with 20 mM phosphate buffer, pH 7.0.) For peptide 16, the amount of buffer was scaled to the amount of peptide, so that at x_p = 0.005 we used 95 μL and at x_p = 0.0323 we used 300 μL. The samples were mixed by hand, with a small glass stirring rod, in the 25 mm long, 8-mm diameter NMR tubes. The NMR experiments typically took from 3 to 4 days for each sample. The samples were checked for degradation by thin-layer chromatography before and after each NMR run. We have found that phospholipid samples are far more stable against hydrolysis in neutral buffer than in distilled water, and there was no indication of phospholipid degradation in any of the samples.

NMR samples containing DPPC-d_{62} and peptide 24 were prepared at the following peptide molar concentrations: x_p

= 0.0051 (lipid to peptide ratio, 196:1), 0.0100 (99:1), 0.0149 (66:1), 0.0197 (50:1), 0.0243 (40:1), and 0.0323 (30:1). For peptide 16, the following concentrations were prepared: x_p = 0.0050 (200:1), 0.0099 (100:1), 0.0149 (66:1), 0.0244 (40:1), and 0.0323 (30:1). In addition, the NMR experiments were repeated on the pure DPPC-d_{62} in phosphate buffer. The pure lipid results are in excellent agreement with those previously published on DPPC-d_{62} (Davis, 1979).

Ideally, all of the NMR experiments should have been performed under identical conditions. For the first two samples studied, peptide 24 at concentrations x_p = 0.0100 and 0.0197, 3.0-μs-long 90° pulses were used to form the quadrupolar echo (Davis et al., 1976) for temperatures where there was evidence of a gel phase component to the spectrum. Instrumental improvements allowed us to use 2.0-μs 90° pulses for all other samples. At the lowest temperatures, the spectrum is quite sensitive to the pulse length (Davis, 1979). However, in ths two-phase region or just below, the spectrum is much less sensitive to pulse length so that we had no trouble performing the spectral subtractions.

The shape of the spectrum is also somewhat sensitive to the time between the two 90° pulses (Davis, 1983; Griffin, 1981). For present purposes, it is sufficient to hold the pulse spacing, τ, constant and to assume that the echo decay, at a given temperature, is the same for all gel phase domains, regardless of sample composition, and similarly for all fluid phase domains at that temperature. We do not require that all parts of the spectrum, whether fluid or gel, have the same echo decay time, T_{2e}. For peptide 24, τ was kept constant at a value of 35 μs. For the peptide 16 series, we used τ = 45 μs. Finally, the recovery time between scans was 0.9 s for all spectra. All other NMR methods are as previously described (Davis, 1979, 1983; Davis et al., 1983). The measurements were made in a superconducting magnet at a frequency of 41.3 MHz.

The temperature for each of the different samples was adjusted to match within 0.1 °C that of all the other samples so that direct comparison under "isothermal" conditions could be made. Reproducibly setting the temperature is especially important when trying to map out the phase boundaries using difference spectroscopy since small differences in temperature can lead to substantial changes in the fluid phase component of the NMR spectrum.

Samples for differential scanning calorimetry were prepared from the same lipid–peptide mixtures used for NMR (M. R. Morrow, J. C. Huschilt, and J. H. Davis, unpublished results). In addition, for some of the NMR samples, part was put into 2-mm-diameter capillary tubes and studied by small-angle X-ray diffraction. These experiments demonstrated that the samples were in a lamellar phase throughout the temperature and composition ranges studied.

Moment analysis and spectral subtractions were performed on an Intel Series II (Intel Corp., Santa Clara, CA) microcomputer development system which was interfaced to a slave microcomputer used for data acquisition. The subtractions were performed in real time by varying the fraction, K, of the second spectrum which was to be subtracted from the first, using a potentiometer, while viewing the difference spectrum on the display screen. In this fashion, it was easy to estimate the uncertainty in the fraction K by inspection of the difference spectrum (Huschilt, 1984).

RESULTS

The chain melting transition in pure DPPC-d_{62} in excess buffer can be regarded as isothermal (Albon & Sturtevant, 1978; Ulmius et al., 1977). The ^{2}H NMR spectrum of phospholipids which are ^{2}H labeled on the hydrocarbon chains

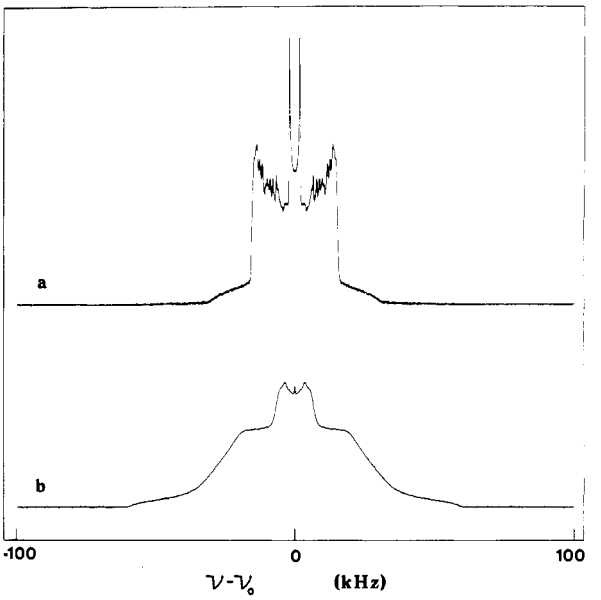

FIGURE 1: Comparison of the ^{2}H NMR spectra of DPPC-d_{62} in excess buffer at (a) 37.5 °C, within the L_α or fluid phase, and at (b) 37 °C, within the $P_{\beta'}$ or gel phase.

is sensitive to this gel to "fluid" transition. For 1,2-bis(perdeuteriopalmitoyl)-*sn*-glycero-3-phosphocholine (DPPC-d_{62}) in excess water or neutral buffer, this transition occurs at about 37.3 °C, and we estimate that it is narrower than about 0.25 °C (Davis, 1979; Davis et al., 1983). The fluid phase spectrum (Figure 1a) covers a frequency range of approximately ±30 kHz about the ^{2}H Larmor frequency while the gel phase spectrum (Figure 1b) extends out to about ±63 kHz. The fluid phase powder pattern spectrum is characterized by numerous sharp 90° edges, a narrow methyl group component with a splitting of only a few kilohertz, and a strong "plateau" in the variation of quadrupolar splitting with chain position. This plateau gives rise to the strong 90° edge at about ±13 kHz in the fluid phase spectrum (Davis, 1979). The gel phase, on the other hand, has a methyl group powder pattern with a splitting of about 14 kHz, while the methylenes exhibit a broad bell-shaped spectrum. The tremendous contrast between these two types of spectra makes it easy to identify the presence and to quantify the amount of each phase under conditions where they coexist.

The difference between these two types of spectra is due to the greatly increased motional averaging that occurs above the chain melting transition. The fluid phase spectrum is characteristic of the rapid axially symmetric molecular motions occurring in that phase. The shape of the gel phase spectrum is determined by the much slower, nonaxially symmetric motions occurring in the gel phase (Griffin, 1981; Meier et al., 1983; Davis, 1983).

The temperature dependence of the ^{2}H NMR spectrum of a 66:1 molar ratio DPPC-d_{62}–peptide 24 sample in excess buffer is shown in Figure 2. At higher temperatures, 38 °C and above, the spectra are characteristic of the fluid phase. As the temperature is lowered, within the fluid phase, from 50 to 38 °C, there is a significant broadening of the spectrum, as seen in the pure lipid (Davis, 1979). This effect, due to increased motional averaging as the temperature is lowered, is clearly evident in the plot of the first moment (M_1) of the spectrum (which for systems with axial symmetry is proportional to the average quadrupolar splitting) as a function of temperature, shown in Figure 3. Values of M_1 are presented for the different concentrations of peptide 16 in Figure 3a and of peptide 24 in Figure 3b. As the peptide 24 concentration

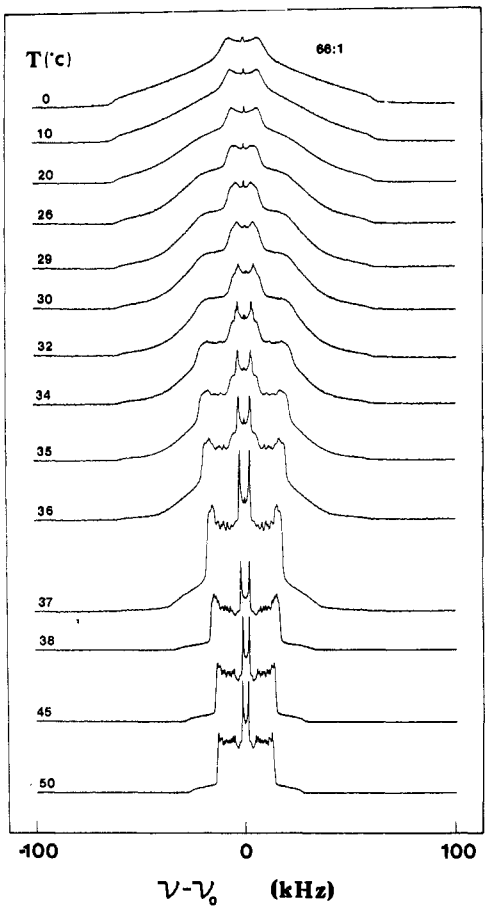

FIGURE 2: Temperature dependence of the ^2H NMR spectrum of the peptide 24–DPPC-d_{62} sample at molar peptide concentration x_p = 0.0149 (mole ratio 66:1). The temperature for each spectrum is displayed on the left.

is increased, there is a clear, monotonic increase in the value of M_1 at each temperature within the fluid phase. For peptide 16, the trend is not so clear.

At 32 °C and below, the spectra in Figure 2 are characteristic of the phospholipid gel phase (Figure 1b) (Davis, 1979). The subtle changes occurring in the methyl group contribution to the spectrum, within ±7 kHz of the center of the spectrum, are typical of the pretransition region of DPPC (Davis, 1979; Westerman et al., 1982). The value of M_1 at temperatures below 32 °C decreases with increasing peptide concentration for both peptides.

Between 30 and 38 °C, the spectra in Figure 2 are superpositions of two components, one from lipids in gel phase domains and the other from fluid domains. As the temperature is lowered within this two-phase region, the gel phase component of the spectrum increases at the expense of that of the fluid phase.

In the presence of peptide, the isothermal chain melting transition, which corresponds to the crossing of a three-phase line in the DPPC–H_2O temperature–composition plot (Ulmius et al., 1977), broadens into a two-phase region where fluid and gel domains coexist in thermodynamic equilibrium. The two-phase lines, which are the boundaries of the two-phase region, both lie below the pure lipid transition temperature. By inspection of the ^2H NMR spectra, such as those in Figure 2, it is possible to locate the temperatures at which the phase boundaries occur for each peptide concentration studied. In the example shown, a DPPC-d_{62} to peptide 24 ratio of 66:1, the boundaries, or two-phase lines, lie between 38 and 37 °C and between 31 and 30 °C. By varying the sample concentration, it is possible using this technique of "nuclear magnetic calorimetry" to map out the phase boundaries in a temperature–composition plot.

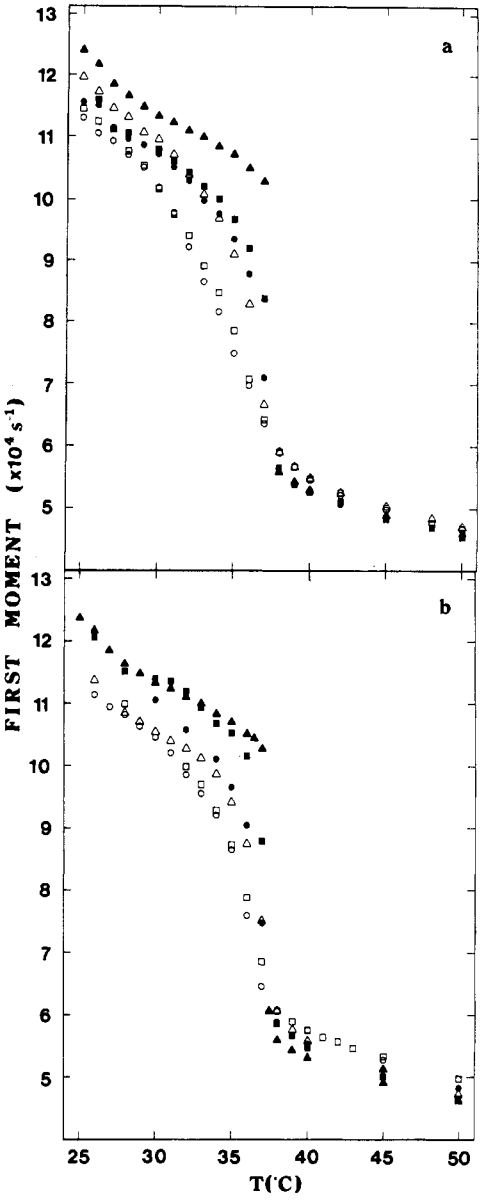

FIGURE 3: Temperature dependence of the first moment of the ^2H NMR spectrum at different concentrations of (a) peptide 16 [(▲) pure lipid, (■) x_p = 0.00498, (●) x_p = 0.00991, (△) x_p = 0.0149, (□) x_p = 0.0244, (○) x_p = 0.0323] and (b) peptide 24 [(▲) pure lipid, (■) x_p = 0.00507, (●) x_p = 0.00997, (△) x_p = 0.0149, (□) x_p = 0.0197, and (○) x_p = 0.0243].

Examining the spectra for different concentrations of peptide at a constant temperature, for example, the 35 °C spectra of the peptide 24–DPPC-d_{62} sample shown in Figure 4, it is again possible to identify the two components of the spectrum and follow them across the two-phase region as the peptide concentration is increased.

The pure lipid spectrum shows that this sample is in the gel phase at 35 °C. The sample whose DPPC-d_{62}:peptide 24 ratio is 196:1 (its actual peptide 24 concentration is x_p = 0.0051) is in the two-phase region at this temperature. This sample is predominantly in the gel phase, but there is a small fraction in fluid domains. A rough estimate of approximately 10% fluid phase can be made on the basis of the relative areas of the fluid and gel phase components of the spectrum.

At a DPPC-d_{62}:peptide 24 ratio of 99:1 (x_p = 0.0100), the spectrum indicates that the fraction of the sample which is

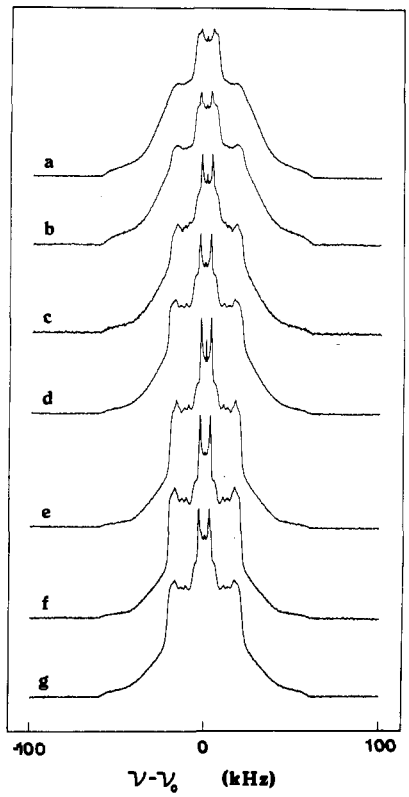

FIGURE 4: Concentration dependence of the ^2H NMR spectrum of peptide 24–DPPC-d_{62} at 35 °C: (a) pure lipid, (b) x_p = 0.00507, (c) x_p = 0.00997, (d) x_p = 0.0149, (e) x_p = 0.0197, (f) x_p = 0.0243, and (g) x_p = 0.0323.

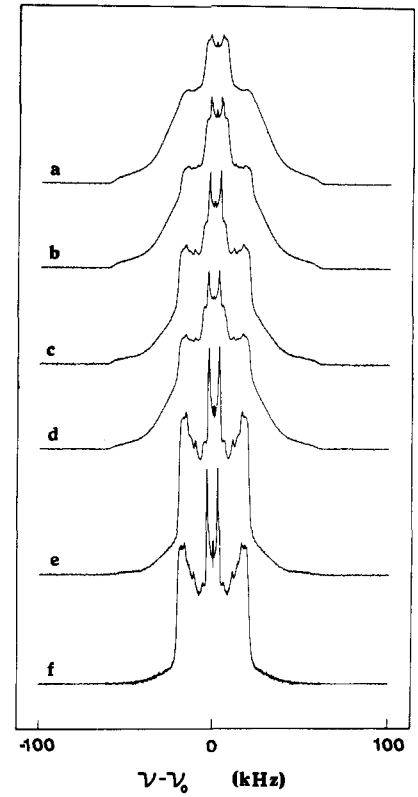

FIGURE 5: Concentration dependence of the ^2H NMR spectrum of peptide 16–DPPC-d_{62} at 35 °C: (a) pure lipid, (b) x_p = 0.00498, (c) x_p = 0.00991, (d) x_p = 0.0149, (e) x_p = 0.0244, and (f) x_p = 0.0323.

in the fluid phase is considerably larger than it was at x_p = 0.0051. This reflects the fact that this concentration is located more deeply within the two-phase region; i.e., it is further away from the phase boundary or two-phase line separating the gel phase from the two-phase region.

As the peptide 24 concentration is increased, the relative area of the fluid phase component of the spectrum increases while that of the gel phase decreases. At sufficiently high peptide concentration, we would eventually cross the phase boundary into the fluid phase. For the highest concentration of peptide 24 which was used, this had not yet occurred at 35 °C, although it does occur at 36 °C. However, this same concentration range with the shorter peptide, peptide 16, does completely traverse the two-phase region at 35 °C, as shown in the spectra of Figure 5.

We can identify, at fixed peptide concentration, the temperature where the phase boundaries are crossed and the concentrations, at fixed temperature, at which phase boundaries are crossed through changes in the spectra. From Figure 5, we can estimate that the gel phase boundary at 35 °C lies between x_p = 0 and x_p = 0.0051 and that the fluid phase boundary lies between x_p = 0.0243 and x_p = 0.0323.

When the NMR spectra are as sensitive to phase changes as these ^2H NMR spectra are to the gel to fluid lipid phase transition, this simple procedure can be a valuable method for mapping out regions of the phase diagram. In the present case, a much more quantitative analysis of the spectra can be performed, yielding an accurate temperature–composition diagram.

Analysis of Difference Spectra. In temperature–composition plots of simple two-component systems, one-phase regions such as our lipid–peptide fluid phase, or the lipid–peptide gel phase, must be separated by a two-phase region where fluid and gel coexist in thermodynamic equilibrium. As we increase peptide concentration, x, from zero along the isotherm at a temperature, T, below the chain melting transition of the pure lipid, T_m, the system is in the gel phase until we reach the two-phase line at concentration $x_g(T)$. Any further increase in peptide concentration results in the conversion of a fraction, $f(T)$, of the system from the gel to the fluid phase. By the lever rule (Moore, 1972; Adamson, 1973)

$$f(T) = [x - x_g(T)]/[x_f(T) - x_g(T)] \quad (1)$$

is the fluid fraction at concentration x and temperature T where $x_f(T)$ and $x_g(T)$ are the concentrations at which the isotherm at temperature T intersects the two-phase lines or boundaries of this two-phase region.

As the concentration is increased within the two-phase region, the fraction of fluid phase increases while the gel phase fraction, $g(T) = 1 - f(T)$, decreases. Thermodynamically, this process corrsponds to the growth of macroscopic fluid phase domains at the expense of gel phase domains. The intrinsic properties of the two types of domains do not change as we cross the two-phase region while the extrinsic properties change linearly with $f(T)$ in accordance with the lever rule.

The technique of nuclear magnetic resonance is a microscopic tool in that the NMR spectrum is sensitive to molecular orientation, order, and dynamics. Furthermore, like other spectroscopic techniques, NMR has an intrinsic time scale, typically on the order of the inverse of the width of the spectrum. The spectrum presents an average over the motions or molecular reorientations that are much faster than this characteristic time scale and is strongly sensitive to motions occurring near this time scale. To the extent that the NMR spectrum can accurately report on the macroscopic behavior of the system, it can be used to study thermodynamic properties such as phase equilibria.

The ^2H NMR spectra of the fluid and gel phases of DPPC-d_{62} (Figure 1) are very different. The widths of the features within these spectra cover a range of from about 1 to 100 kHz, resulting in a range of time scales from about 10μs to 1 ms.

The ^2H NMR spectrum from a sample of concentration x at a temperature within the two-phase region will consist of two distinguishable components, one gellike and the other fluid-like, provided that exchange of DPPC-d_{62} molecules between gel and fluid domains is slow on the ^2H NMR time scale. The sharpest feature in the spectrum, the fluid phase methyl group resonance, has a $T_{2e} \simeq 1$ ms (Davis, 1979). Motions faster than, or on the order of, this time scale can influence the shape of the spectrum. The decay time for the quadrupolar echo, T_{2e}, is in many ways analogous to the T_2 of high-resolution NMR lines. Just as T_2 determines the line width of the high-resolution peak, T_{2e} can dominate the quadrupolar echo spectrum if $1/T_{2e}$ is greater than the contribution of the magnet inohomogeneity to the line width. This typically occurs in our system when $T_{2e} \lesssim 10$ ms. Near the fluidus boundary, gel phase domains may be small so that diffusion between domains could lead to an averaged spectrum. For this effect to be negligible, it is sufficient that the gel domains have an area greater than $\pi\langle r^2\rangle_{gel} \sim 10^4$ Å^2, corresponding to domains with more than or on the order of 200 phospholipids on each side of the bilayer since each lipid occupies approximately 60 Å^2 (Seelig, 1981; Levine & Wilkins, 1971).

At the other side of the two-phase region, near the solidus curve, the fluid phase domains may be small. In this case, because of the much faster diffusion rate in the fluid phase, the domains would need to have an area greater than $\pi\langle r^2\rangle_{fluid} \sim 10^6$ Å^2, corresponding to approximately 20 000 phospholipids. The efficiency of the exchange (or conversion) between gel and fluid phase lipids at the domain boundaries will also influence the averaging process, so that even when domains are smaller than these estimates, we may not see evidence of interdomain diffusion in the spectra. As the peptide concentration is varied at a fixed temperature within the two-phase region, the size and number of gel phase domains can be expected to vary. Near the end points, i.e., near the phase boundaries, we might expect to see some effect of this exchange process on the spectrum. In fact, there is no clear evidence for exchange between domains in any of our ^2H NMR spectra.[2] In the absence of this process, the ^2H NMR spectra should accurately represent the partitioning of the system between gel and fluid.

An important assumption we make is that the quadrupolar echo decay time, T_{2e}, and the component spectra (characteristic of the end points) behave as intrinsic properties of the system, i.e., that they are independent of x_p within the two-phase region at fixed temperature. The experimental spectra at x_p and T within the two-phase region will then faithfully represent the end-point spectra, the relative fraction of each being give by the lever rule.

[2] Exchange between fluid and gel phase domains would broaden the sharp fluid phase peaks in the spectrum. At all concentrations and temperatures near the "fluidus" boundary, these peaks remain sharply defined. Near the "solidus" boundary, it is difficult to be certain, but there is no clear evidence for exchange there. In addition, the description of the spectra in terms of two nonexchanging components is strongly supported by the decomposition of the moments of the composite spectra into the moments of the end-point spectra (eq 6). In all cases, this decomposition is in complete agreement with the positions of the end points determined by spectral subtraction and with the moments of the end-point spectra.

If we can safely ignore exchange between domains, then the spectrum, $F(x_A)$, at concentration x_A and temperature T within the two-phase region is, for $x_A \ll 1$

$$F(x_A,T) \simeq f_A(T)F_f[x_f(T)] + [1 - f_A(T)]F_g[x_g(T)] \quad (2)$$

The temperature, T, is explicitly displayed in eq 2 to emphasize that the concentrations at the phase boundaries depend on temperature but not on sample contentration. The fluid fraction, $f_A(T)$, depends on temperature and on peptide concentration. Equation 2 simply states that the spectrum at concentration x_A and temperature T, within the two-phase region, consists of a superposition of a fluid phase component, F_f, characteristic of domains at concentration $x_f(T)$, and a gel phase component, F_g, characteristic of gel phase domains at concentration $x_g(T)$. With $F(x_A)$, $F_f(x_f)$, and $F_g(x_g)$ all normalized, the fluid fraction $f_A(T)$ is proportional to the amount of fluid phase domains, and $1 - f_A(T)$ is proportional to the amount of gel phase domains.

In a similar fashion, the spectrum at concentration x_B and temperature T consists of a superposition of the same two end-point spectra, $F_f(x_f)$ and $F_g(x_g)$, but the amount of each will be different, varying according to the lever rule. In general, at a concentration x_i within the two-phase region, the spectrum at temperature T will be given by

$$F(x_i,T) = \frac{x_i - x_g(T)}{x_f(T) - x_g(T)}F_f(T) + \frac{x_f(T) - x_i}{x_f(T) - x_g(T)}F_g(T) \quad (3)$$

The nth moment of the spectrum, M_n, is defined by

$$M_n(x_i,T) = \int_0^\infty \omega^n F(x_i,T;\omega)\, d\omega \Big/ \int_0^\infty F(x_i,T;\omega)\, d\omega \quad (4)$$

where now the frequency dependence of the NMR spectrum, $F(x_i,T;\omega)$, is shown explicitly. Inserting eq 3 into eq 4 gives

$$M_n(x_i,T) = f_i(T)M_n^f(T) + [1 - f_i(T)]M_n^g(T) \quad (5)$$

so that the moments as well as the spectra can be used to extract information on the partitioning of the sample between the two phases. Indeed, the moments of the experimental spectra within the two-phase region at fixed temperature vary linearly with x_p according to the lever rule and are in complete agreement with the results of the spectral subtractions.

The ^2H NMR spectra at concentrations x_A and x_B and temperature T are both superpositions of the same end-point spectra. In this example, $x_A < x_B$ so that subtracting a fraction K of the spectrum at x_B, $F(x_B,T)$ from the spectrum at x_A, $F(x_A,T)$ gives

$$\begin{aligned} &F(x_A,T) - KF(x_B,T) = \\ &f_AF_f(T) + (1 - f_A)F_g(T) - K[f_BF_f(T) + (1 - f_B)F_g(T)] = \\ &\qquad (f_A - Kf_B)F_f(T) + (1 - K - f_A + Kf_B)F_g(T) \end{aligned} \quad (6)$$

We obtain the gel phase end-point spectrum, $F_g(T)$, when $f_A - KF_B = 0$ or $K = f_A/f_B < 1$. Then

$$F(x_A,T) - KF(x_B,T) = (1 - K)F_g(T) \quad (7)$$

Similarly, subtracting a fraction K' of the spectrum at x_A from that at x_B gives

$$\begin{aligned} &F(x_B,T) - K'F(x_A,T) = \\ &f_BF_f(T) + (1 - f_B)F_g(T) - K'[f_AF_f(T) + (1 - f_A)F_g(T)] = \\ &\qquad (f_B - K'f_A)F_f(T) + (1 - K' - f_B + K'f_A)F_g(T) \end{aligned}$$

We obtain the fluid phase end-point spectrum $F_f(T)$ when $1 - f_B = K'(1 - f_A)$ or $K' = (1 - f_B)/(1 - f_A) < 1$. Then

$$F(x_B,T) - K'(x_A,T) = (f_B - K'f_A)F_f(T) \quad (8)$$

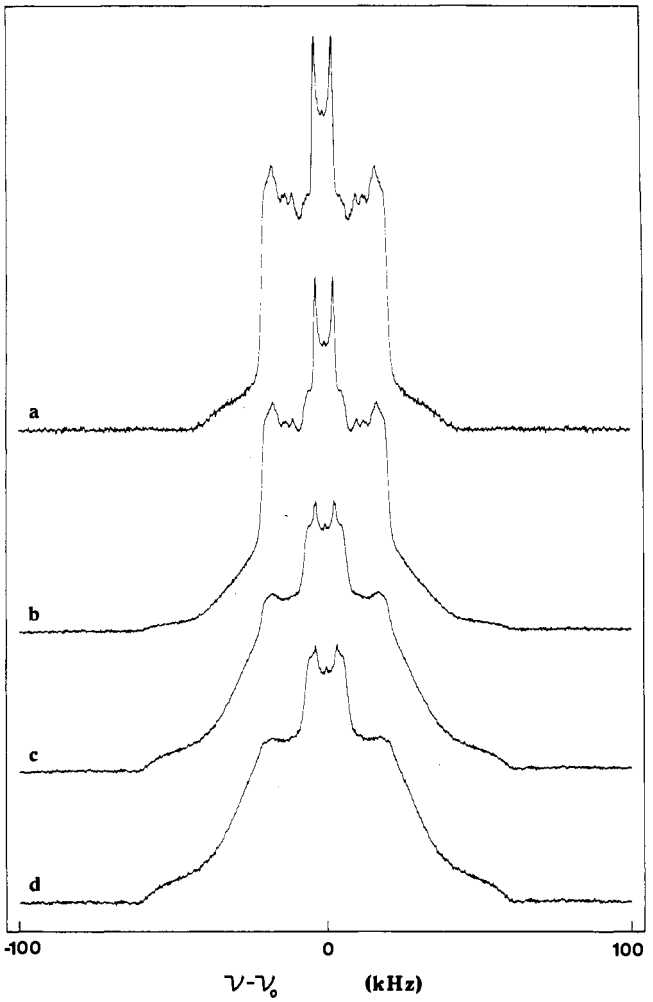

FIGURE 6: Extraction of the two end-point spectra from two spectra at the same temperature but different concentrations within the two phase region. This example is for peptide 24 at 35 °C: (a) fluid phase end-point spectrum at $x_F = 0.0383$; (b) two-component spectrum at $x_p = 0.0243$; (c) two-component spectrum at $x_p = 0.0051$; (d) gel phase end-point spectrum at $x_g = 0.0003$. The spectrum in (a) was obtained by subtracting the fraction 0.42 times the spectrum in (c) from that in (b). The spectrum in (d) was obtained by subtracting the fraction 0.20 times that in (b) from that in (c).

Figure 6 shows the difference spectra $F_f(T)$ and $F_g(T)$ obtained at $T = 35$ °C by using the experimental spectra at peptide 24 concentrations $x_A = 0.0051$ (196:1 lipid:peptide ratio) and $x_B = 0.0243$ (40:1 lipid:peptide ratio).

The value of K' is determined by varying the fraction of $F(x_A,T)$ subtracted from $F(x_B,T)$ until the spectral intensity in the difference spectrum at frequencies from about 50 to 60 kHz from the central frequency, i.e., beyond the shoulders in the fluid phase component, is zero and the base line in that region is flat. If too much is substracted, this part of the spectrum goes negative; if too little, positive intensity remains. In this fashion, K' can be determined quite accurately, and its relative uncertainty, typically less than 10%, can be estimated. For the spectra in Figure 6, the fluid phase end-point spectrum is obtained with $K' = 0.42 \pm 0.02$.

Determining the value of K which gives the gel phase end-point spectrum is more difficult so that the relative error is somewhat larger than for K'. This involves subtracting a fraction of $F(x_B,T)$ from $F(x_A,T)$ until the sharp spectral features characteristic of the fluid phase disappear from the difference spectrum. If too large a fraction of $F(x_B,T)$ is subtracted from $F(x_A,T)$, then the difference spectrum will show sharp negative features. If not enough is subtracted,

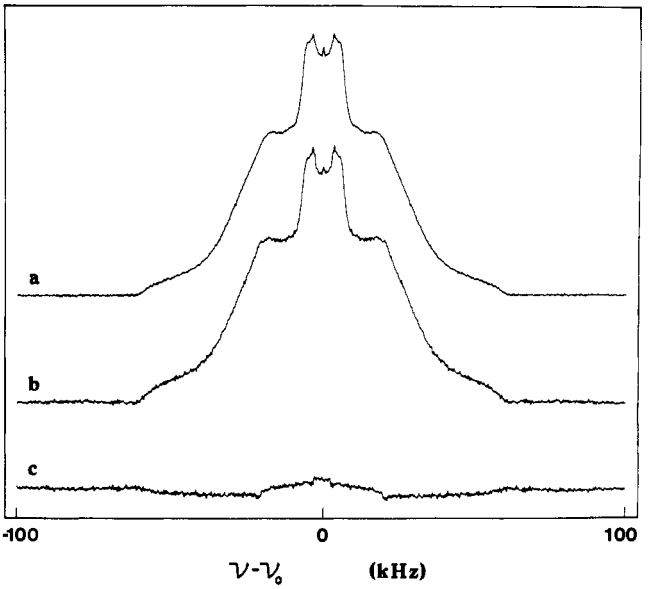

FIGURE 7: Comparison of (a) the pure lipid gel phase ^2H NMR spectrum with (b) the gel phase end-point spectrum from Figure 6. The difference between (a) and (b) is shown in (c).

small, sharp positive features will still be present. The prominent sharp features to watch during the subtraction are the narrow methyl group edges and the sharp 90° edge characteristic of the fluid phase plateau (Davis, 1979). The spectra in Figure 6 give a value of $K = 0.20 \pm 0.05$.

The pure lipid gel phase spectrum at 35 °C is compared to the end-point difference spectrum in Figure 7. Clearly, the major features of the spectrum of the $P_{\beta'}$ phase lipid (Figure 7a) are present in the difference spectrum (Figure 7b). [This observation is consistent with the calorimetric data (M. R. Morrow, J. C. Huschilt, and J. H. Davis, unpublished results) since the pretransition persists in the presence of these peptides.] The difference spectrum is that of the gel phase at a finite peptide concentration x_g so that it is not expected to be identical with that of the pure lipid. The difference between the two spectra in Figure 7a,b is shown in Figure 7c.

The values of K and K' with which the end-point spectra have been obtained can also be used to give the peptide concentrations at the end points. Using the lever rule

$$x_g = \frac{f_B x_A - f_A x_B}{f_B - f_A} = \frac{x_A - K x_B}{1 - K} \tag{9}$$

and

$$x_f = \frac{x_B - K' x_A}{1 - K'} \tag{10}$$

For our example at 35 °C (Figure 6), $x_g = 0.003 \pm 0.002$ and $x_f = 0.038 \pm 0.002$.

Any two spectra at different concentrations but the same temperature within the two-phase region can be used to obtain the end-point concentrations and end-point spectra. For any two concentrations x_i and x_j, within the two-phase region at a common temperature T, where we take $x_i > x_j$, we have

$$1 - K' = \frac{x_i - x_j}{x_f - x_j} \tag{11}$$

By performing pairwise subtractions for all possible pairs x_i and x_j, and using eq 10, we can obtain the weighted average value of x_f. For example, at 35 °C for peptide 24, there are spectra for 6 concentrations within the two-phase region so that there are 15 distinct combinations. The values of x_f

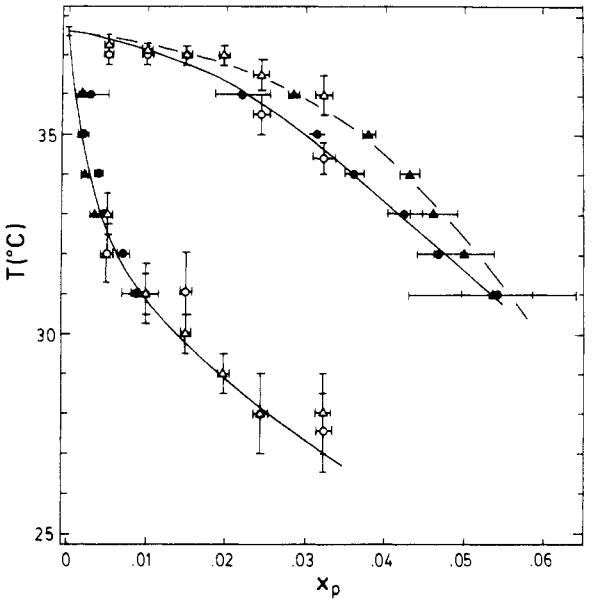

FIGURE 8: Temperature–composition plots of the two peptide–lipid systems. The triangles refer to peptide 24 and the circles to peptide 16. The open symbols were obtained by visual inspection of series of spectra as in Figure 2. In these cases, the horizontal error bars represent the uncertainties in sample concentrations and the vertical error bars the uncertainty in the temperature where two components in the spectra can be identified. The solid symbols were obtained by spectral subtraction and represent the average values of the end-point concentrations. The horizontal error bars represent the uncertainties in these values.

determined by these subtractions are averaged to give $\langle x_f \rangle = 0.0380 \pm 0.0008$. The uncertainty is simply the weighted root mean squared deviation from the mean value (i.e., the standard deviation). The weights are inversely proportional to the square of the uncertainty in K'. The values of x_g determined by the reverse procedure leading to gel phase end-point spectra are averaged in the same way, using eq 9, to give, for peptide 24 at 35 °C, $\langle x_g \rangle = 0.0018 \pm 0.0006$.

Discussion

In this manner, finding the difference end-point spectra for all pairwise combinations as a function of temperature, we obtain the temperature–composition plots for the two peptides, as shown in Figure 8. The circles are for peptide 16, and the triangles are for peptide 24. Open symbols are the temperatures at the phase boundaries as determined by inspection of the temperature sequences of spectra at each sample concentration. The vertical error bars on the open symbols represent the estimated uncertainty in determining the boundaries from a series of spectra taken at 1 °C intervals. The horizontal error bars on these symbols are the uncertainties in the sample concentrations.

The solid symbols are the values of x_f and x_g obtained by spectral subtraction at each temperature for which there were more than two sample concentrations within the two-phase region. The horizontal error bars on the solid symbols are the uncertainty in the values of x_f and x_g.

The solid curves were simply sketched in to help identify the phase boundaries for the peptide 16 system, and correspondingly, the dashed curves are for the peptide 24 system.

The phase diagrams of the two peptide–lipid systems are similar in that both peptides induce the formation of a two-phase region at temperatures below the pure lipid melting point. The two-phase line (fluidus curve) separating the fluid phase from the mixed phase region for the shorter peptide lies below that for the longer peptide. The two peptides we have used differ only in their length. Peptide 16 has a hydrophobic core of 16 leucines, which in an α-helix would have a length of 2.4 nm, while the 24-leucine core of peptide 24 has an α-helical length of 3.6 nm. The shorter peptide more closely matches the hydrophobic thickness of the fluid phase lipid bilayer so that it should favor the formation of the fluid phase more than peptide 24. However, the fluidus curve for peptide 16 is, at most, only 1 or 1.5 °C below that of peptide 24, and the two-phase lines (solidus curves) separating the gel phase from the two-phase region do not differ significantly. Therefore, when the peptide has a hydrophobic length which is slightly greater than or approximately equal to the hydrophobic thickness of the fluid phase bilayer, a slight mismatch has an observable but not an overwhelming effect on the phase behavior of the system. We have not yet tested the significance of a hydrophobic mismatch in the case where the peptide is significantly shorter than the fluid phase bilayer thickness. The mattress model of Mouritsen & Bloom (1984) parameterizes the peptide–lipid interaction in terms of this mismatch and seems capable of predicting the observed phase behavior. The present data, however, do not seem to be sufficient to provide a test of this model.

Moment analysis, eq 4 and 5, of the end-point spectra shows that as we move along the fluidus curve toward higher peptide concentration and lower temperatures the average quadrupolar splitting, or first moment, gradually increases. The end-point spectra retain the characteristic shape of the pure phospholipid. It is not possible to separate the effects of increasing peptide concentration and decreasing temperatures on these end-point spectra, however.

In the fluid phase of the samples with peptide 24, we noted an increase in the first moment as the peptide 24 concentration was increased (Figure 3). The fact that this effect is present with peptide 24 but not with peptide 16 may be due to the tendency of the longer peptide to increase the bilayer thickness, thereby straightening the hydrocarbon chains and increasing the average quadrupolar splitting (Davis et al., 1983). In comparison, earlier studies on reconstituted systems, cytochrome *c* oxidase in 1-palmitoyl-2-palmitoleoyl-*sn*-glycero-3-phosphocholine (Paddy et al., 1981) and rhodopsin in 1,2-dimyristoyl-*sn*-glycero-3-phosphocholine (Bienvenue et al., 1982), found no significant change in the value of the first moment as the protein concentration was increased within the fluid phase. By nearly matching the fluid phase bilayer thickness peptide 16 mimics more closely the behavior of membrane proteins.

Examination of Figure 3a,b at temperatures between 25 and 37 °C reveals that the shorter peptide (Figure 3a) has a greater disordering effect than peptide 24. Presumably, this is due to the greater mismatch between the length of the shorter peptide and the gel phase bilayer thickness.

The phase diagram provides a complete description of how lipid and peptide partition between phases. For example, the mole fraction of peptide in the fluid phase, i.e., n_p^f/n_p (the number of moles of peptide in fluid phase domains divided by the total number of moles of peptide) is given by

$$\frac{n_p^f}{n_p} = \frac{x_f}{x_p} f \tag{12}$$

where f is the fluid fraction (eq 1). This quantity is plotted for $x_p \simeq 0.01$ for peptide 16 in Figure 9. The solid circles are the values determined from $\langle x_f \rangle$ and $\langle x_g \rangle$. The smooth curve was obtained from the solid curve sketched on the phase diagram of Figure 8. This behavior should be contrasted with the temperature dependence of the fluid fraction, f, at the same

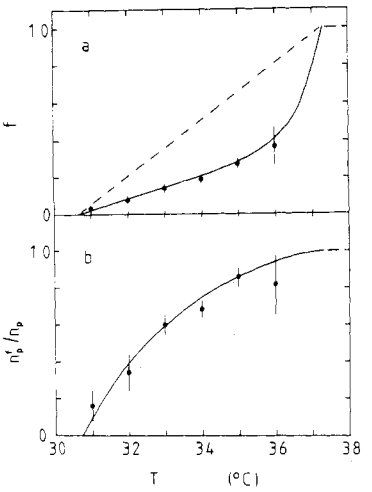

FIGURE 9: (a) Fluid fraction, f, as a function of temperature for peptide 16 at $x_p = 0.00991$. The dashed curve is what would have been obtained if the sample had melted uniformly or linearly as the temperature was increased through the two-phase region. (b) Mole fraction of peptide 16 in the fluid phase, n_n^f/n_p, vs. temperature. The solid curves in both (a) and (b) correspond to the solid curves sketched in as phase boundaries in Figure 8. The error bars are calculated from the uncertainties in x_f and x_g as given in Figure 8.

concentration, shown in Figure 9. While the total sample melts relatively slowly as the temperature is raised, the peptide enters the fluid phase much more rapidly. For example, for peptide 16 at 32.5 °C, the fluid fraction $f \simeq 0.11$, while $n_p^f/n_p \simeq 0.50$. Only 11% of the total sample is fluid, but 50% of the peptide is in those fluid domains.

The ability to measure the distribution of membrane proteins among available phases is a prerequisite to the construction of quantitative models to explain the temperature dependence of membrane protein activity. Accurate measurement of this partitioning of the protein, coupled with accurate measurements of the temperature dependence of protein activity, will provide a meaningful description of the influence that physical properties of the membrane have on protein function (Thilo et al., 1977; Silvius & McElhaney, 1982). In particular, it should be possible to accurately determine the relative activities of proteins in the two phases.

Conclusion

We have described a method of determining phase boundaries by ^2H NMR difference spectroscopy. This approach is applicable to situations where the spectra of the component phases are significantly different, as occurs with the model membrane's fluid and gel phases. On the basis of previous work on reconstituted systems, specifically cytochrome *c* oxidase–1-palmitoyl-2-palmitoleoyl-*sn*-glyerco-3-phosphocholine (Paddy et al., 1981) and rhodopsin–1,2-dimyristoyl-*sn*-glycero-3-phosphocholine (Bienvenue et al., 1982), we anticipate that the method will have wide applicability.

The phase boundaries which we have determined by NMR contain information which is complementary to that accessible by differential scanning calorimetry. The results obtained by using these two techniques on our peptide–lipid systems are sufficient to construct a simple thermodynamic model describing the phase behavior.

Acknowledgments

We thank Drs. M. Bloom, F. W. Dahlquist, K. R. Jeffrey, A. L. MacKay, and M. R. Morrow for many valuable discussions.

Registry No. DPPC, 2644-64-6; peptide 16, 94751-61-8; peptide 24, 86968-49-2.

References

Adamson, A. W. (1973) *A Textbook of Physical Chemistry*, Academic Press, New York.

Albon, N., & Sturtevant, J. M. (1978) *Proc. Natl. Acad. Sci. U.S.A. 75*, 2258–2260.

Bienvenue, A., Bloom, M., Davis, J. H., & Devaux, P. F. (1982) *J. Biol. Chem. 257*, 3032–3038.

Blume, A., Rice, D. M., Wittebort, R. J., & Griffin, R. G. (1982) *Biochemistry 21*, 6220–6230.

Brophy, P. J., Horvath, L. L., & Marsh, D. (1984) *Biochemistry 23*, 860–865.

Chapman, D., Gômez-Fernândez, J. C., & Goñi, F. M. (1979) *FEBS Lett. 98*, 211–223.

Davis, J. H. (1979) *Biophys. J. 27*, 339–358.

Davis, J. H. (1983) *Biochim. Biophys. Acta 737*, 117–171.

Davis, J. H., Jeffrey, K. R., Bloom, M., Valic, M. I., & Higgs, T. P. (1976) *Chem. Phys. Lett. 42*, 390–394.

Davis, J. H., Hodges, R. S., & Bloom, M. (1982) *Biophys. J. 37*, 170–171.

Davis, J. H., Clare, D. M., Hodges, R. S., & Bloom, M. (1983) *Biochemistry 22*, 5298–5305.

Deese, A. J., Dratz, E. A., Dahlquist, F. W., & Paddy, M. R. (1981) *Biochemistry 20*, 6420–6427.

Fahey, P. F., & Webb, W. W. (1978) *Biochemistry 17*, 3046–3053.

Griffin, R. G. (1981) *Methods Enzymol. 72*, 108–174.

Griffith, O. H., Brotherus, J. R., & Jost, P. C. (1982) *Lipid–Protein Interactions* (Jost, P. C., & Griffith, O. H., Eds.) Vol. 2, pp 225–238, Wiley, New York.

Gupta, C. M., Radhakrishnan, R., & Khorana, H. G. (1977) *Proc. Natl. Acad. Sci. U.S.A. 74*, 4315–4319.

Huschilt, J. C. (1984) Masters Thesis, University of Guelph, Guelph, Ontario, Canada.

Jacobs, R. E., & Oldfield, E. (1981) *Progress in NMR Spectroscopy* (Emsley, J. W., Feeney, J., & Sutcliffe, L. H., Eds.) Pergamon Press, Oxford.

Jost, P., Griffith, O. H., Capaldi, R. A., & Vanderkooi, G. (1973) *Proc. Natl. Acad. Sci. U.S.A. 70*, 480–484.

Kang, S. Y., Gutowsky, H. S., Hshung, J. C., Jacobs, R., King, T. E., Rice, D., & Oldfield, E. (1979) *Biochemistry 18*, 3257–3267.

Levine, Y. K., & Wilkins, M. F. H. (1971) *Nature (London), New Biol. 230*, 69.

Lewis, B. A., & Engelman, D. M. (1983) *J. Mol. Biol. 166*, 203–210.

Mabrey, S., & Sturtevant, J. M. (1976) *Proc. Natl. Acad. Sci. U.S.A. 73*, 3862–3866.

McLachlan, A. D., & Henderson, R. (1980) *Biochem. Soc. Trans. 8*, 677–678.

Meier, P., Ohmes, E., Kothe, G., Blume, A., Weidner, J., & Eibl, H. J. (1983) *J. Phys. Chem. 87*, 4904.

Moore, W. J. (1972) *Physical Chemistry*, Prentice-Hall, Engelwood Cliffs, NJ.

Mouritsen, O., & Bloom, M. (1984) *Biophys. J. 46*, 141–153.

Oldfield, E., Gilmore, R., Glaser, M., Gutowsky, H. S., Hshung, J. C., Kang, S. Y., King, T. E., Meadows, M., & Rice, D. (1978) *Proc. Natl. Acad. Sci. U.S.A. 75*, 4657–4660.

Owichi, J. C., & McConnell, H. M. (1979) *Proc. Natl. Acad. Sci. U.S.A. 76*, 4750–4754.

Owicki, J. C., Springgate, M. W., & McConnell, H. M. (1978) *Proc. Natl. Acad. Sci. U.S.A. 75*, 1616–1619.

Paddy, M. R., Dahlquist, F. W., Davis, J. H., & Bloom, M.

(1981) *Biochemistry 20*, 3152–3162.
Seelig, J. (1981) *Membranes and Intercellular Communication* (Balian, R., Chabre, M., & Devaus, P. F., Eds.) pp 18–78, North-Holland, Amsterdam.
Silvius, J. R., & McElhaney, R. N. (1982) *Rev. Infect. Dis. 4*, S50–S57.
Sixl, F., Brophy, P. J., & Watts, A. (1984) *Biochemistry 23*, 2032–2039.
Thilo, L., Träuble, H., & Overath, P. (1977) *Biochemistry 16*, 1283–1290.
Ulmius, J., Wennerstrom, H., Lindblom, G., & Arvidson, G. (1977) *Biochemistry 16*, 5742–5745.
Westerman, P. W., Vaz, M. J., Strenk, L. M., & Doane, J. W. (1982) *Proc. Natl. Acad. Sci. U.S.A. 79*, 2890–2894.

Spin-Label Studies of Lipid–Protein Interactions in (Na^+,K^+)-ATPase Membranes from Rectal Glands of *Squalus acanthias*

Mikael Esmann,[‡] Anthony Watts,[§,∥] and Derek Marsh*[,§]

Max-Planck-Institut für biophysikalische Chemie, Abteilung Spektroskopie, D-3400 Gottingen, Federal Republic of Germany, and Institute of Biophysics, University of Aarhus, DK-8000 Aarhus, Denmark
Received July 12, 1984

ABSTRACT: Lipid–protein interactions in (Na^+,K^+)-ATPase-rich membranes from the rectal gland of *Squalus acanthias* have been studied by using spin-labeled lipids in conjunction with electron spin resonance (ESR) spectroscopy. Lipid–protein associations are revealed by the presence of a second component in the ESR spectra of the membranes in addition to a component which corresponds very closely to the ESR spectra obtained from dispersions of the extracted membrane lipids. This second component corresponds to spin-labeled lipids whose motion is very significantly restricted relative to that of the fluid lipids in the membrane or the lipid extract. A stoichiometry of approximately 66 lipids per 265 000-dalton protein is found for the motionally restricted component of those spin-labeled lipids (e.g., phosphatidylcholine) which show least specificity for the protein. This corresponds approximately to the number of lipids which may be accommodated within the first shell around the $\alpha_2\beta_2$ protein dimer. A selectivity of the various spin-labeled lipids for the motionally restricted component associated with the protein is found in the following order: cardiolipin > phosphatidylserine ≈ stearic acid ≳ phosphatidic acid > phosphatidylglycerol ≈ phosphatidylcholine ≈ phosphatidylethanolamine ≈ androstanol.

(Na^+,K^+)-ATPase (EC 3.6.3.1) is a transport enzyme which pumps sodium antiport to potassium coupled to ATP hydrolysis. A highly enriched membranous preparation is obtainable from the rectal gland of *Squalus acanthias* (Skou & Esmann, 1979) in which the ATPase is present as an integral membrane protein associated with much of its endogenous lipid. The active form of the enzyme is an $\alpha_2\beta_2$ dimer of molecular weight 265 000 (Esmann et al., 1980), similar to findings on the enzyme obtained from other sources. A topic of considerable interest is the interaction of the (Na^+,K^+)-ATPase with its membrane lipid environment.

Electron spin resonance (ESR)[1] spin-label studies have shown that large integral membrane proteins are capable of appreciably restricting the mobility of the lipid chains in contact with the hydrophobic surface of the protein [for a review, see Marsh & Watts (1982)]. On the one hand, a charge selectivity has been demonstrated in the interaction of single-chain spin-labels with (Na^+,K^+)-ATPase preparations from *Electrophorus electricus* (Brotherus et al., 1980). On the other hand, a head-group selectivity has been found in the interaction of spin-labeled phospholipids with cytochrome oxidase (Knowles et al., 1981) and several other integral membrane proteins (Marsh, 1985). In the present study, we investigate the interaction of a series of different spin-labeled phospholipids with the (Na^+,K^+)-ATPase from *Squalus acanthias*. A marked selectivity is observed for various phospholipid head groups, indicating a specific interaction with certain phospholipids, namely, phosphatidylserine, phosphatidic acid, and cardiolipin. From measurements of the nonspecific interactions, it is possible to estimate the total number of lipid molecules in contact with the intramembranous surface of the (Na^+,K^+)-ATPase.

Materials and Methods

(Na^+,K^+)-ATPase-rich membranes were prepared from the rectal gland of *Squalus acanthias* according to the method of Skou & Esmann (1979) but omitting treatment with saponin. Typically, the (Na^+,K^+)-ATPase constituted about 70% of the total membrane protein, and the specific activity was 1500 μmol of P_i mg^{-1} h^{-1}. The preparation contained 5–6 mol of residual deoxycholate per mol of enzyme (1 mol of deox-

[‡] University of Aarhus. Supported by the Danish Medical Research Council and the "Ingeborg and Leo Dannin's Foundation for Medical Research".
[§] Max-Planck-Institut für biophysikalische Chemie.
[∥] Present address: Department of Biochemistry, University of Oxford, Oxford OX1 3QU, U.K.

[1] Abbreviations: ESR, electron spin resonance; *n*-SASL, *n*-(4,4-dimethyloxazolidine-*N*-oxyl)stearic acid; *n*-PASL, *n*-PESL, *n*-PCSL, *n*-PSSL, and *n*-PGSL, 1-acyl-2-[*n*-(4,4-dimethyloxazolidine-*N*-oxyl)-stearoyl]-*sn*-glycero-3-phosphoric acid, -phosphoethanolamine, -phosphocholine, -phosphoserine, and -phosphoglycerol, respectively; 14-CLSL, 1-(3-*sn*-phosphatidyl)-3-[1-acyl-2-[14-(4,4-dimethyloxazolidine-*N*-oxyl)stearoyl]glycero-3-phospho]-*sn*-glycerol; ASL, 17β-hydroxy-4′,4′-dimethylspiro[15α-androstane-3,2′-oxazolidin]-3′-yloxy; CDTA, *trans*-1,2-diaminocyclohexane-*N*,*N*,*N*′,*N*′-tetraacetic acid; DMPC, dimyristoylphosphatidylcholine.

0006-2960/85/0424-1386$01.50/0